Int. J. Solids Structures Vol. 18, No. 8, pp. 643–658, 1982
Printed in Great Britain.

0020-7683/82/080643-16$03.00/0
Pergamon Press Ltd.

INFLUENCE OF STRAIN HARDENING ON THE DEFORMATION OF THIN RINGS SUBJECTED TO OPPOSED CONCENTRATED LOADS

S. R. REID and W. W. BELL

Department of Engineering, University of Aberdeen, Aberdeen AB9 1AS, Scotland

(*Received* 7 *January* 1982)

Abstract—Experiments in which metal rings are compressed to large deflections by a pair of opposed concentrated loads reveal a load-deflection characteristic which is at variance with the simple theory based upon rigid-perfectly plastic behaviour. This problem is analysed using a model which incorporates strain hardening in an approximate fashion and it is shown how the discrepancies between the experiments and the simple theory arise. The results of the theory are presented in non-dimensional form and it is shown that the varieties of response depend upon the value of the parameter $mR = (6\sigma_0 R/E_p h)^{1/2}$. The results relate to early work concerned with the effects of strain hardening on the post-collapse behaviour of frame structures and they are compared with similar analyses of rings crushed between flat plates.

INTRODUCTION

In plastic buckling problems the strain hardening properties of the structural material play a key role, see for example [1–3]. However, apart from such problems, the effect of strain hardening on the response of a structure beyond the load at which plastic "collapse" occurs according to limit analysis has been given little attention and this is particularly so where gross deformation is involved. Such considerations are of importance in the field of impact energy absorption where one is often concerned with the design of metallic structural components and systems to dissipate large amounts of kinetic energy as they deform plastically to large deflections. A number of such components have been reviewed by Johnson and Reid[4].

Metal tubes provide a very adaptable component for use in this way and several aspects of their response to loading conditions leading to gross plastic deformation have been described in the literature [5–10]. During the course of an investigation of the lateral compression of metal tubes/rings between flat plates [11–13] it became clear that the material strain hardening properties play a significant role in defining the shape of the load-deflection curve. A relatively simple method of incorporating the effect of strain hardening into a theoretical model for tube crushing was described by Reid and Reddy [11]. In this model the plastic hinges at which the major deformation occurred were replaced by plastic regions. This enabled the interaction between changes in geometry and strain hardening to be examined in some detail. It transpired that the shape of the non-dimensionalised load-deflection curve was governed by the parameter mR defined by

$$mR = (6\sigma_0 R/E_p h)^{1/2} \tag{1}$$

where σ_0 and E_p are the yield stress and mean strain-hardening modulus of the material used and R and h are the tube radius and wall-thickness respectively. When a tube is crushed between flat plates it has a monotonically increasing load-deflection curve, a fact which greatly simplifies the solution of the governing equations [11].

Interest in the title problem stems from a number of sources. Single rings/tubes have been incorporated into crash barriers for bridge rails [9] and it is clear that their loading condition lies somewhere between flat plate compression and diametrically opposed point loading. An understanding of the response to the latter type of loading would therefore complement the earlier study in aiding a better appreciation of the response of this energy absorbing element. Secondly, from the theoretical point of view, the problem is a more complex one than flat plate compression. The rigid-perfectly plastic analysis of the problem based on the four hinge mode of collapse shown in Fig. 1(a) gives the load P and the deflection δ at a certain stage of the

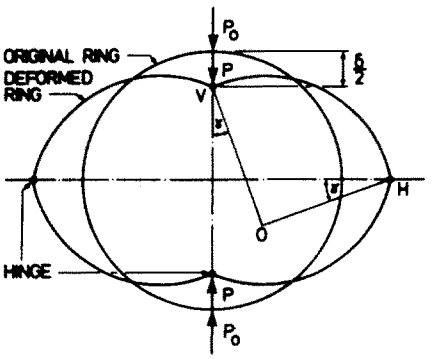

(a)

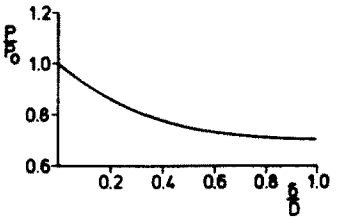

(b)

Fig. 1.(a) Rigid-perfectly plastic mode of collapse of point-loaded ring. (b) Non-dimensional load-deflection curve from eqn (4).

deformation in terms of the angle γ as

$$P = \frac{P_0}{\cos\gamma + \sin\gamma} \tag{2}$$

and

$$\delta = D(1 + \sin\gamma - \cos\gamma), \tag{3}$$

where $P_0 = (4M_0/R)$ is the initial collapse load for the ring which has diameter $D(=2R)$ and is assumed to have unit length. M_0, the fully plastic bending moment per unit length of ring, is equal to $\sigma_0 h^2/4$. Equations (2) and (3) can be combined to give

$$P = \frac{P_0}{\left[1 + 2\left(\frac{\delta}{D}\right) - \left(\frac{\delta}{D}\right)^2\right]^{1/2}} \tag{4}$$

and a graph of (P/P_0) against (δ/D), the non-dimensional load-deflection curve, is given in Fig. 1(b). The response according to rigid-plastic theory is therefore unstable in the sense that the load reduces with increasing deflection.

To a certain extent this behaviour has been borne out in the results of some recent tests in which thin mild steel rings and short tubes were loaded by diametrically opposed conically-headed punches [14]. In these tests the main concern was the interaction between overall structural response and the onset of penetration and subsequent fracture under the punch. However it was noted that for short rings (having a length to diameter ratio of less than 1.5) a "knee-shaped" transition occurred between initial plastic collapse and significant plastic deformation. The load invariably rose over a certain deflection range before eventually falling in a manner reminiscent of Fig. 1(b) although off-set from it by a significant amount. The rings usually fractured after this phase as the ultimate tensile strength was reached at the most heavily stressed points. Tests in which specimens were loaded incrementally and annealed at the end of each increment [14], showed that the load-deflection curve predicted by the rigid

perfectly plastic theory, eqn (4), could be reproduced approximately by annihilating the effects of strain hardening. A similar conclusion was reached by Reddy and Reid [13] for tubes compressed between flat plates.

That strain hardening can remove an instability of the sort described above, i.e. a decreasing load-deflection curve, was noted by Onat [15] in an early discussion of second order effects associated with the plastic collapse analysis of frames. In a sense the approach described below represents a continuation of his approach into the realm of gross deformations.

BEHAVIOUR OF VARIOUS POINT-LOADED RINGS

In order to illustrate the range of shapes of the load-deflection curve of a ring compressed diametrally by opposed point loads, a few preliminary tests were performed on mild steel and aluminium rings using an Instron Universal testing machine. In contrast to the experiments reported in [14] the rings tested were all 12.5 mm long and were compressed between knife edges which extended over their entire length. This reduced the tendency for penetration to occur under the load point.

Four sets of data are presented in Fig. 2(a–d). In each case the point load data is accompanied by the results of a flat-plate compression test on an identical specimen and the rigid-plastic curve of Fig. 1(b) suitably scaled for the particular specimen. In each case the deflection is shown as a fraction of the diameter. Figure 2(a) relates to an as-received mild steel ring of 89 mm outside diameter and 3.2 mm wall thickness. In common with most of the characteristics of ring specimens described in [14], fracture intervened before the ring could be compressed to deflections much in excess of half its diameter. It clearly shows however a falling load-deflection curve which starts soon after the point of initial collapse. Figure 2(b) shows the behaviour of an annealed mild steel ring of 89 mm outside diameter and 1.6 mm wall thickness. After the onset of plastic collapse the load reduces at a slow rate until a deflection ratio of 0.4 is reached at which point the load begins to increase. Figure 2(c) shows the behaviour of an annealed specimen which is otherwise identical to that shown in Fig. 2(a), i.e. 89 mm outside diameter and 3.2 mm wall thickness. There is no evidence of the load reducing at all with this specimen; rather it increases gradually to a load which is about 13% higher than the initial collapse load at a deflection ratio of 0.8. Finally Fig. 2(d) shows the behaviour of an annealed

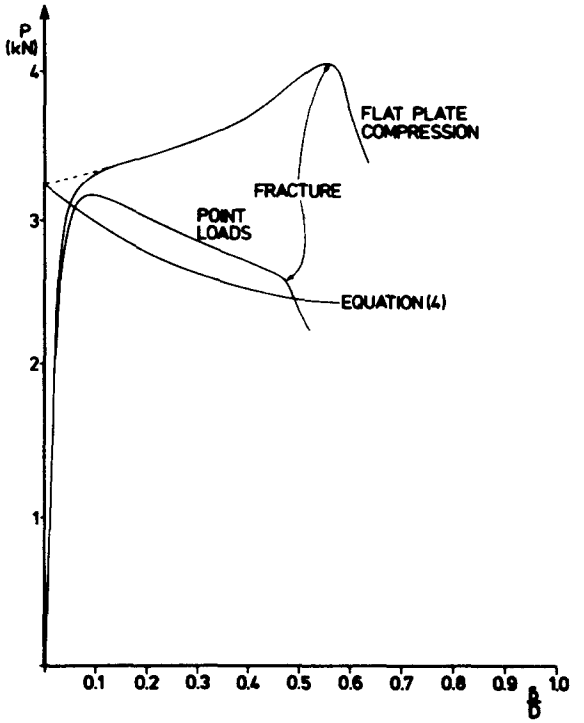

Fig. 2(a).

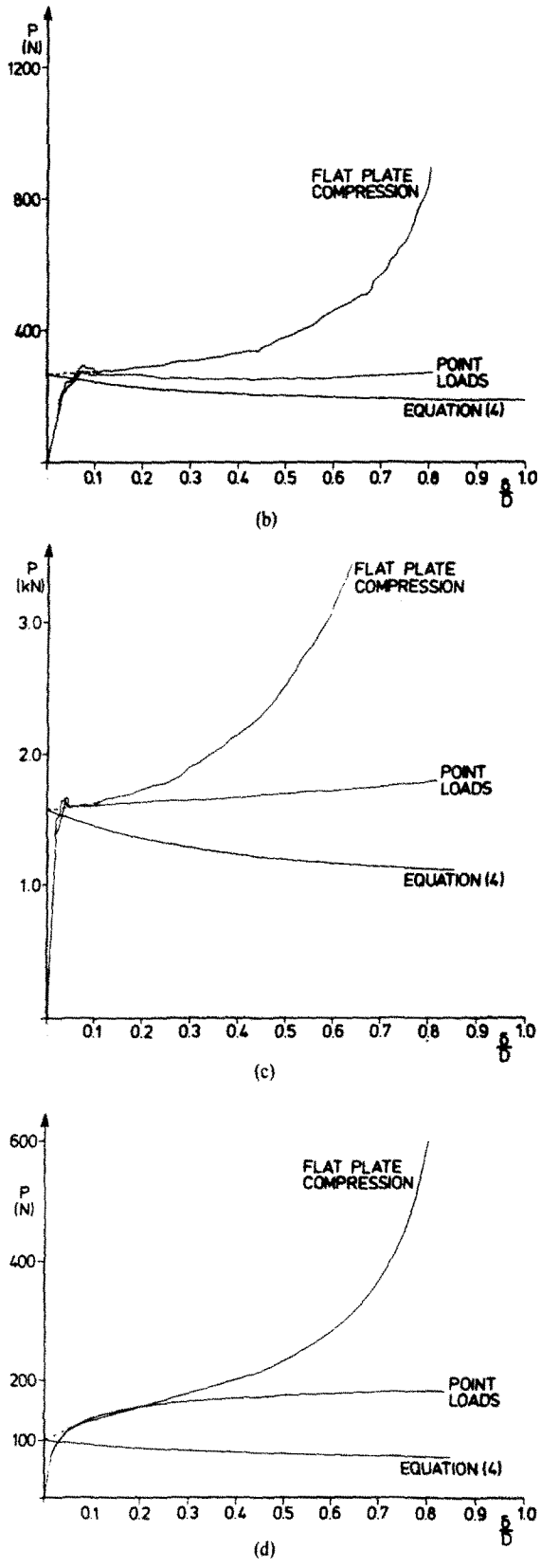

Fig. 2. Comparison between load-deflection curves for rings compressed between flat plates, by opposed point loads and the prediction of eqn (4). (a) As-received mild steel ring, outside diameter 89 mm, wall thickness 3.2 mm. (b) annealed mild steel ring, outside diameter 89 mm, wall thickness 1.6 mm. (c) annealed mild steel ring, outside diameter 89 mm, wall thickness 3.2 mm. (d) annealed aluminium ring, outside diameter 50 mm, wall thickness 1.6 mm.

aluminium ring of 50 mm outside diameter and 1.6 mm wall thickness. The definition of a collapse load for this material is somewhat more tenuous than for mild steel because of its more rounded stress-strain curve (this is discussed further below) but, taking a value of 100 N, Fig. 2(d) shows that the load increases by approximately 80% when the ring has been compressed to a deflection ratio of 0.8. This is dramatically different from the prediction given by eqn (4).

These results will be discussed later in the light of the theoretical model described in the next section.

BASIS OF PROPOSED MODEL

The approach adopted for the analysis of the deformation of a ring between opposed point loads is broadly the same as that described in [11] for compression of a ring between flat plates. In [11] only the concentrated hinges at the ends of the horizontal diameter were replaced by regions which deformed according to the strain hardening moment-curvature relationship

$$|\kappa| = \begin{cases} \dfrac{|M| - M_0}{E_p I} & |M| > M_0 \\ 0 & |M| < M_0 \end{cases} \tag{5}$$

where κ is the change in curvature, E_p is the strain hardening modulus (assumed constant) and $I = h^3/12$, the ring being assumed to have unit length. For a number of reasons [13] the concentrated hinges at the edge of the plate contact region were retained in the earlier work. Clearly in the present problem it would be inconsistent to model the region around H in this way and not replace the hinge at V by a similar plastic region. Consequently it is assumed that the structural elements of a quadrant of the ring are as shown in Fig. 3.

The centreline of the arc HV is assumed to be inextensible and HB and AV are plastic regions which deform according to eqn (5). They behave essentially as elasticas of flexural rigidity E_pI (hence the term plastica coined in [13]). AB is a rigid circular arc which has undergone rigid body motion. Its current orientation is defined by the angles ψ_A and θ_B shown in Fig. 3(b) and prior to loading its position was defined by angles α and β shown in Fig. 3(a).

The aim is to calculate the deflection between the load points, δ, in terms of the applied load P. For generality the load-deflection curves and other data are produced in non-dimensional form. A non-dimensional measure of the deflection is given by

$$\frac{\delta}{D} = 1 - (l_1 + l_2 + l_3)/R \tag{6}$$

where l_1, l_2 and l_3 are the vertical projected lengths of the portions HB, BA and AV respectively as shown in Fig. 3(b). The non-dimensional load, λ, is defined by

$$\lambda = \frac{P}{P_0} \tag{7}$$

where P_0 is the rigid-plastic collapse load defined previously. The material properties σ_0 and E_p

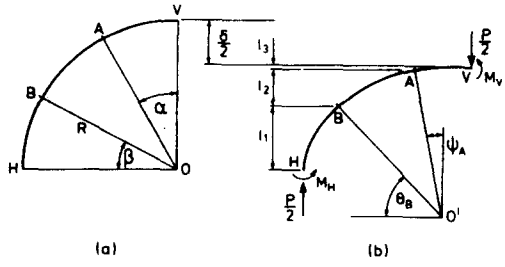

Fig. 3. Structural elements of quadrant of point loaded ring. (a) Geometry prior to deformation. (b) Deformed geometry.

and the geometrical parameters R and h can be combined into two non-dimensional parameters σ_0/E_p and R/h. As will be shown below, it transpires that the solution is governed by the parameter $(6\sigma_0 R/E_p h)^{1/2}$ which was denoted by mR in [11] and this notation will be retained herein.

ANALYSES OF ARCS *HB* AND *AV*

Using intrinsic co-ordinates (θ,s) for HB and (ψ,t) for AV we deduce from Fig. 4 and eqn (5) the following governing equations:

$$\frac{d^2\theta}{ds^2} = -k^2 \sin\theta \quad \text{for} \quad HB \tag{8}$$

$$\frac{d^2\psi}{dt^2} = k^2 \cos\psi \quad \text{for} \quad AV \tag{9}$$

where $k^2 = P/2E_pI$. These equations will be considered separately.

Arc HB

Integrating eqn (8) leads to

$$\frac{1}{2}\left(\frac{d\theta}{ds}\right)^2 = k^2 \cos\theta + C,$$

where C is a constant of integration. Using $(d\theta/ds) = (1/R)$ at $\theta = \theta_B$ gives

$$\frac{d\theta}{ds} = \frac{1}{R}\{1 + 2k^2R^2(\cos\theta - \cos\theta_B)\}^{1/2}. \tag{10}$$

We note that the expression k^2R^2 appearing in this equation and in subsequent ones can be written in terms of λ and mR since

$$k^2R^2 = \lambda(mR)^2. \tag{11}$$

The length of HB is given by $R\beta$ thus

$$\beta = \frac{1}{R}\int_0^{\theta_B} \frac{ds}{d\theta}\,d\theta = \int_0^{\theta_B} \{1 + 2\lambda m^2R^2(\cos\theta - \cos\theta_B)\}^{-1/2}\,d\theta$$

$$= \frac{1}{\lambda^{1/2}mR} F(\phi_B,p) \tag{12}$$

where

$$p^2 = \tfrac{1}{2}\left(1 - \cos\theta_B - \frac{1}{2\lambda m^2R^2}\right), \qquad \sin\phi_B = \frac{1}{p}\sin\frac{\theta_B}{2}$$

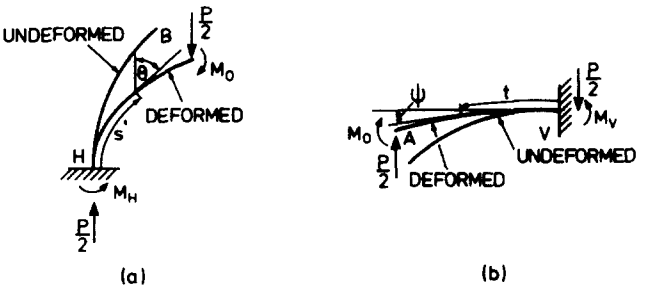

Fig. 4.(a) Loads and co-ordinate system for region *HB*. (b) Loads and co-ordinate system for region *AV*.

and F is the incomplete elliptic integral of the first kind. The length l_1 shown in Fig. 3(b) is given by

$$\frac{l_1}{R} = \frac{1}{R}\int_0^{\theta_B} \frac{ds}{d\theta}\cos\theta\, d\theta$$

$$= \int_0^{\theta_B} \{1 + 2\lambda m^2 R^2(\cos\theta - \cos\theta_B)\}^{1/2}\cos\theta\, d\theta$$

$$= \frac{1}{\lambda^{1/2} mR}\{2E(\phi_B, p) - F(\phi_B, p)\} \tag{13}$$

where E is the incomplete elliptic integral of the second kind.

Arc AV

The analysis of the deformation of arc AV is somewhat similar to that above but has an added complication. A point of inflection within the arc may occur so that $(d\psi/dt)$ is no longer necessarily of a single sign throughout. The procedure for dealing with this additional effect is described below. Integrating eqn (9) gives

$$\tfrac{1}{2}\left(\frac{d\psi}{dt}\right)^2 = k^2 \sin\psi + D$$

where D the constant of integration can be written in terms of the non-dimensional curvature at V, κ_v, given by

$$\kappa_v = R\left(\frac{d\psi}{dt}\right)_{\psi=0}.$$

Thus $D = \frac{1}{2}\kappa_v^2/R^2$ and we have

$$\frac{d\psi}{dt} = \pm\frac{1}{R}(\kappa_v^2 + 2\lambda m^2 R^2 \sin\psi)^{1/2}. \tag{14}$$

κ_v plays a key role in the solution procedure below. The boundary condition at A is

$$\left(\frac{d\psi}{dt}\right)_{\psi=\psi_A} = \frac{1}{R}.$$

Thus,

$$1 = \kappa_v^2 + 2\lambda m^2 R^2 \sin\psi_A. \tag{15}$$

Whether we take the positive or negative sign in eqn (14) depends upon the sign of κ_v. If $\kappa_v > 0$ then since $(d^2\psi/dt^2) > 0$ we must have $(d\psi/dt) > 0$ throughout AV and hence

$$\frac{d\psi}{dt} = \frac{1}{R}(\kappa_v^2 + 2\lambda m^2 R^2 \sin\psi)^{1/2}. \tag{16}$$

If $\kappa_v < 0$ then $(d\psi/dt)$ must initially be negative, increase to zero at a point of inflection where $\psi = \psi_I$ and then become positive. Under these circumstances

$$\frac{d\psi}{dt} = \begin{cases} -\dfrac{1}{R}(\kappa_v^2 + 2\lambda m^2 R^2 \sin\psi)^{1/2} & 0 < \psi < \psi_I \\ \dfrac{1}{R}(\kappa_v^2 + 2\lambda m^2 R^2 \sin\psi)^{1/2} & \psi_I < \psi < \psi_A. \end{cases} \tag{17}$$

From eqn (16), ψ_I is given by

$$\kappa_v^2 + 2\lambda m^2 R^2 \sin \psi_I = 0. \tag{18}$$

The following expression gives the angle α which can be thought of as the non-dimensional arc length,

$$\alpha = \frac{1}{R}\int_0^{\psi_A} \frac{dt}{d\psi}\, d\psi$$

$$= \begin{cases} \dfrac{1}{\lambda^{1/2} mR}\{F(\phi^*,q) - F(\phi_A,q)\} & \text{for } \kappa_v > 0 \\ \dfrac{1}{\lambda^{1/2} mR}\left\{2F\left(\dfrac{\pi}{2},q\right) - F(\phi^*,q) - F(\phi_A,q)\right\} & \text{for } \kappa_v < 0 \end{cases} \tag{19}$$

where

$$q^2 = \tfrac{1}{2}\left(1 - \sin \psi_A + \frac{1}{2\lambda m^2 R^2}\right), \tag{19}$$

$$\sin \phi^* = \frac{1}{\sqrt{2}q} \quad \text{and} \quad \sin \phi_A = \frac{1}{q}\sin\left(\frac{\pi}{4} - \frac{\psi_A}{2}\right). \tag{20}$$

Furthermore

$$\frac{l_3}{R} = \frac{1}{R}\int_0^{\psi_A} \frac{dt}{d\psi} \sin \psi\, d\psi$$

$$= \begin{cases} \dfrac{1}{\lambda^{1/2} mR}\{2E(\phi^*,q) - F(\phi^*,q) - 2E(\phi_A,q) + F(\phi_A,q)\} & \text{for } \kappa_v > 0 \\ \dfrac{1}{\lambda^{1/2} mR}\left\{4E\left(\dfrac{\pi}{2},q\right) - 2E(\phi^*,q) + F(\phi^*,q) - 2E(\phi_A,q)\right. & \\ \left. + F(\phi_A,q) - 2F\left(\dfrac{\pi}{2},q\right)\right\} & \text{for } \kappa_v < 0. \end{cases} \tag{21}$$

SYSTEM OF GOVERNING EQUATIONS

Considering the rigid arc AB we can write down the following geometrical compatibility equation,

$$\alpha + \beta = \psi_A + \theta_B. \tag{22}$$

Moment equilibrium for this arc gives

$$\frac{PR}{2}(\cos \theta_B - \sin \psi_A) = 2M_0,$$

which reduces to the following non-dimensional form,

$$\cos \theta_B - \sin \psi_A = \frac{1}{\lambda}.$$

Finally we have

$$\frac{l_2}{R} = \cos \psi_A - \sin \theta_B. \tag{24}$$

This completes the system of equations required to solve the problem. Unlike the problem of the compression of a ring between flat plates [11], the deflection is not a single valued function of the load over the complete range of mR values. It is therefore necessary to utilise a parameter in terms of which both the load factor and the deflection may be calculated uniquely. The curvature κ_v under the load fulfils this role. The solution procedure is to eliminate α and β between eqns (12), (18) and (22). This gives an equation containing ψ_A, θ_B and λ and equation (23) gives a further equation containing these variables. From eqn (15) we have

$$\lambda = \frac{1 - \kappa_v^2}{2m^2R^2 \sin \psi_A} \tag{25}$$

and so λ may be eliminated to give two non-linear equations for ψ_A and θ_B which may be solved numerically for a given value of mR over a range of values of κ_v decreasing from its initial value of unity. The values of ψ_A and θ_B can then be substituted into eqns (13), (21) and (24) to give l_1, l_2 and l_3 and hence, via eqns (25) and (6), λ and (δ/D). Thus the load-deflection curve for a given value of mR can be constructed.

RESULTS

The results of the above theory are presented in non-dimensional form in Figs. 5–7 for a range of mR values. Figure 5 shows the non-dimensional load-deflection curves which change as mR reduces from those in which the load reduces over a large part of the range to curves in which the load increases monotonically, this latter behaviour applying when mR is less than 4 approximately. The theory therefore predicts a range of behaviour which encompasses that observed in the preliminary tests described earlier.

Detailed features of the deformation of a given ring are conveyed in Figs. 6 and 7. Figure 6(a) shows the growth of the plastic zone around V expressed in terms of the increase in the angle α as the deflection increases. The length of the "hinge" around V is $2\alpha R$. Figure 6(b) shows the way in which the curvature κ_v increases with deflection and from it the maximum strain at V can be estimated. Figure 7 provides similar data for the plastic zone around H.

DISCUSSION

Interaction between changes in geometry and strain hardening

When analysing the gross plastic deformation of a metallic structural component, care must

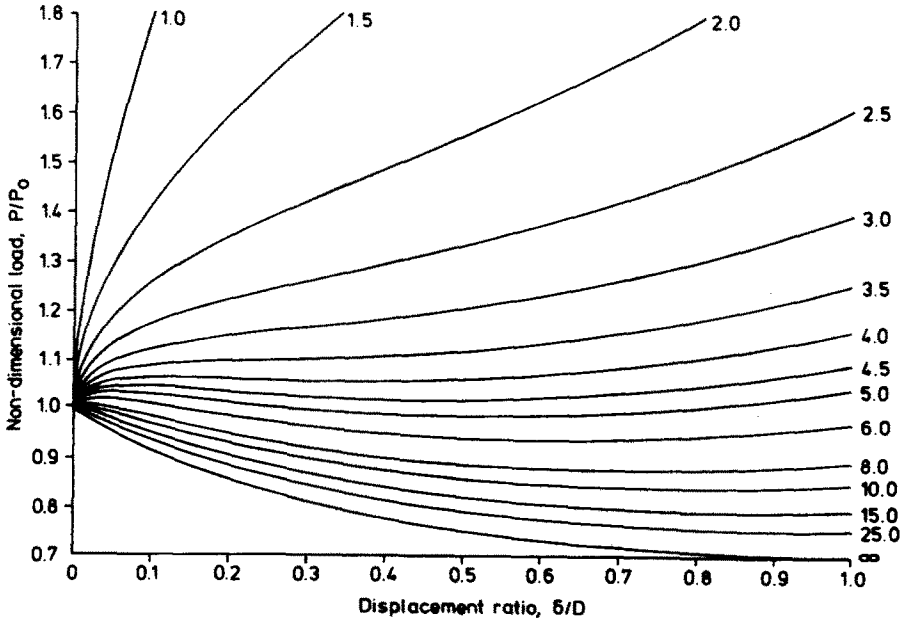

Fig. 5. Non-dimensional load-deflection curves for point loaded rings over a range of mR values.

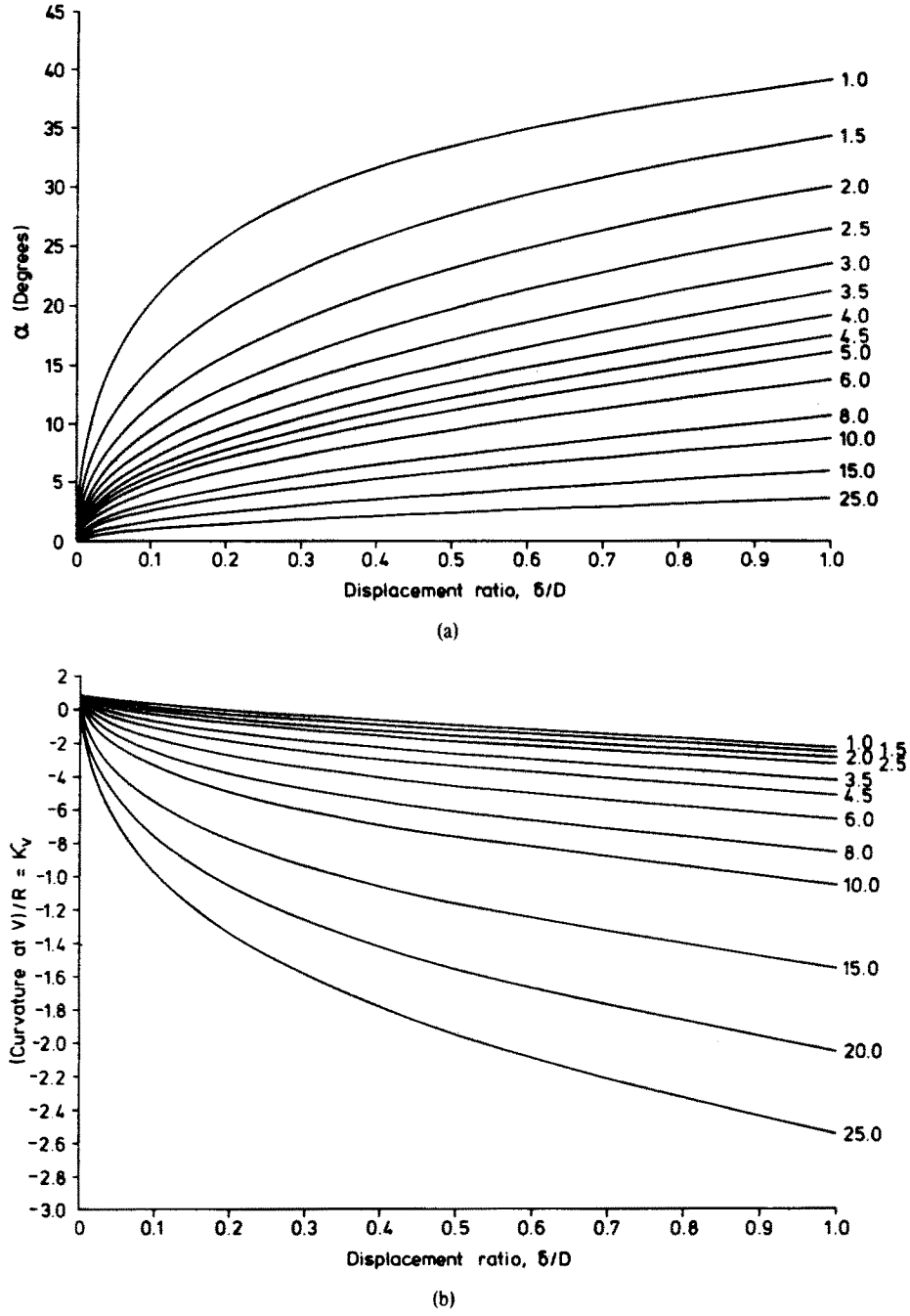

Fig. 6.(a) Non-dimensionalised variation in the length of the region AV with deflection. (b) Non-dimensional curvature at V vs deflection.

be taken to ensure that all the significant effects are given due consideration. The influence of change in geometry is clearly of prime interest and yet, as the analysis above and previous similar studies have shown, a consideration of this alone can produce a model which gives only a crude representation of the behaviour of an actual component. In order to improve the theoretical prediction of the load-deflection characteristic some account must be taken of the effects of strain hardening. Where bending is the principal mode of deformation, gross overall deformation of the component usually implies the localisation of the deformation around those critical portions of structure (plastic hinges) which can be identified through a simple limit analysis. Under these circumstances strain hardening has two main effects. It requires an increase in the bending moment applied to a given cross section if the curvature is changed there and secondly it causes the region undergoing plastic deformation to spread.

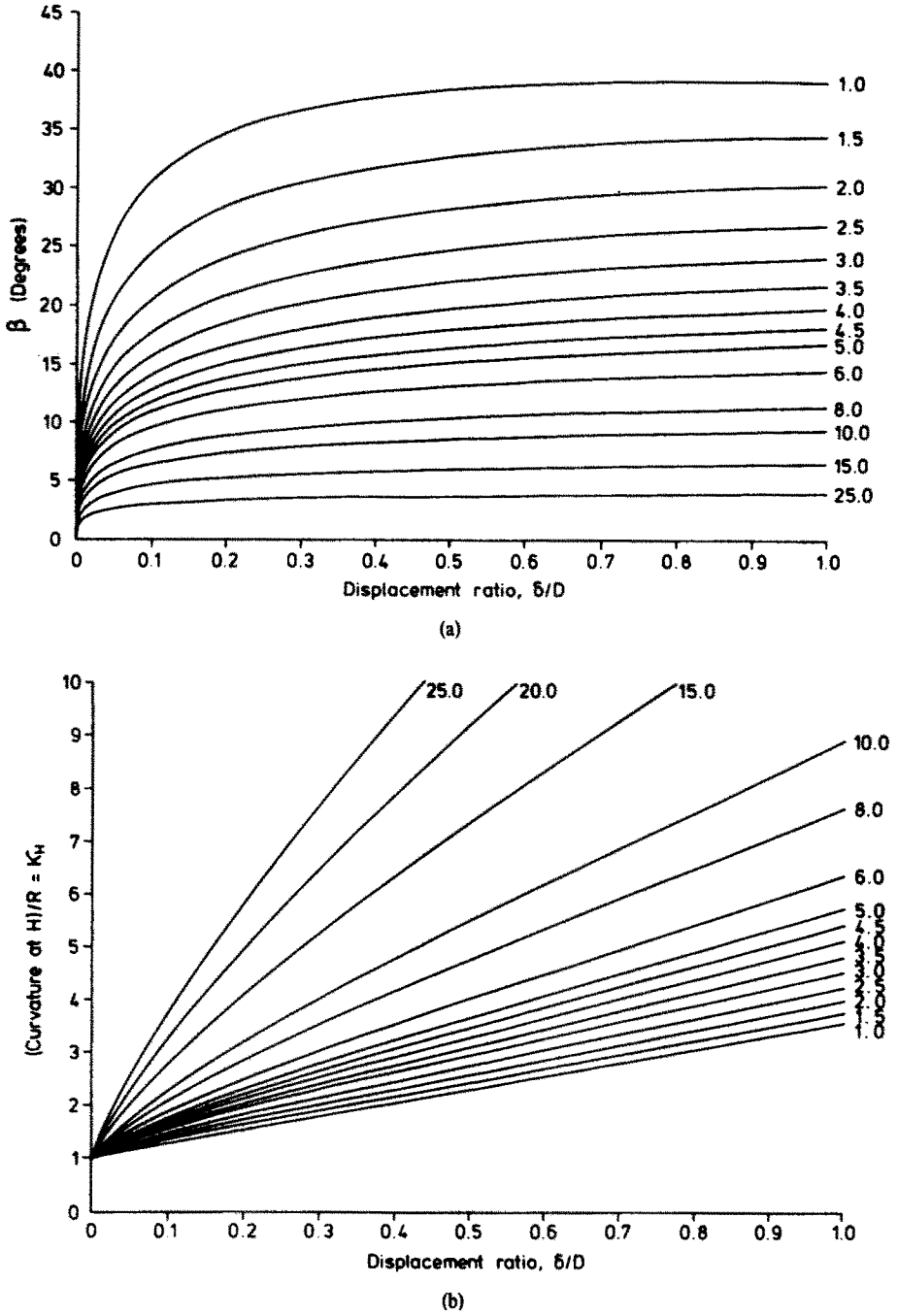

Fig. 7.(a) Non-dimensionalised variation in the length of the region HB with deflection. (b) Non-dimensional curvature at H vs deflection.

In [11] the effects of strain-hardening were incorporated into the analysis of a ring compressed between flat plates although only the regions around H were modelled using the "plastica" theory described above, a limitation which will be discussed in further detail below. When a ring is compressed in this way, the effect of the change in geometry is to reduce the moment arm of the applied force about the plastic hinges. This reduction in the moment arm requires an increase in the applied force in order to continue the deformation. This occurs even when strain hardening is omitted from the analysis but leads to an even more rapid increase in load when strain hardening is included. In the initial stages however the increase in bending moment at the centre of the regions is offset by the fact that the zone of deformation spreads. After a reduction in diameter of approx. 40% (the precise value depending upon the value of

mR in the model) the plastic zone is compelled to reduce in length as the moment arm reduces, the deformation becomes more concentrated and consequently the hardening of the material leads to a noticeable steepening of the load-deflection curve which matches that observed experimentally. Further comments will be made below concerning the relationship between ring response under flat plate compression and that under opposed point loads.

In the problem considered in this paper the change in geometry generally implies an increase in the moment arm so that in the perfectly plastic limit continued deformation occurs under conditions of reducing load; the response is unstable. The inclusion of any degree of strain hardening removes this instability in a manner similar to that discussed for the small deflection of frames by Onat [15]. Initially any deformation involves changes in the curvature at V and H and thus the prevailing bending moment increases at these sections. Simultaneously the length of the regions around H and V spread as shown in Figs. 6(a) and 7(a). The zone around H spreads at a faster rate than that around V and virtually reaches its maximum length at a reduction in diameter of 20–30%. The length of the plastic zone around V increases steadily throughout the deformation. For large values of mR the effect of the increasing moment arm dominates and eventually the load reduces. The slowing down of the spread of the plastic zones leads to increased moments at H and V which then results in an increase in the applied load for values of mR less than 10. The tendency of strain hardening to increase the load directly opposes the effect of the change in geometry and for mR less than 4 it is able to remove the instability completely. This phenomenon is entirely dependent on the interaction between strain hardening and change in geometry and, as can be seen from the results of the experiments described above, reflects the behaviour of actual rings under test. Finally, it is interesting to note that, unlike the case of flat-plate compression (Fig. 9, Ref. [11]), the length of the plastic zone around H does not reduce in length thus indicating that no unloading occurs in this case within the ring.

Comparison between theory and experiments

The basic assumption made in the theoretical model is that the behaviour of the material can be described by a rigid-linear strain hardening law which in turn leads to the moment-curvature relationship given in eqn (5). The neglect of elastic deformation is unlikely to lead to significant errors if the R/h ratio is sufficiently small. With reference to structures used for impact energy absorption this is usually the case. For materials in general however, the assumption of linear strain hardening can at best be considered a crude approximation to the actual material response. The use of this approach for flat plate compression of rings/tubes produced satisfactory agreement between theory and experimental data for mild steel, zircaloy [12], and copper [16] when an average value for the strain hardening modulus was used in the theory. This led to the proposal [12] that ring compression tests could be used to estimate material properties particularly where specimen preparation is either hazardous (for example when the material has been irradiated) or likely to lead to changes in behaviour due to flattening of specimens cut from tube stock.

The collapse load P_0 can be estimated by extrapolating the load-deflection curve back to the load axis as shown in Fig. 2. A non-dimensional load-deflection curve can then be constructed by dividing the loads by P_0 and the deflection δ by the diameter. Plotting this curve on to a family of theoretical $\lambda - \delta/D$ curves covering a range of mR values enables the relevant mR value (or range of values) to be determined for the ring. Using the expressions for P_0 and mR, values for σ_0 and E_p, can be estimated [12]. The success or otherwise of this approach depends upon the variation in E_p over the strain range to which the plastic regions are exposed. This can be seen for the rings compressed in the small selection of tests described above. Figure 8 shows the non-dimensional load-deflection curves for the flat plate compression tests on the four ring specimens considered at two different scales so that the relevant range of mR values for each ring can be identified.

The fact that the data for each ring crosses several of the theoretical curves provided reflects the variation in the mean strain hardening modulus during the deformation. For the as-received mild steel ring the experimental points lie in a region where mR is changing rapidly and hence covers a wide range of values of the order of 20. The behaviour of the ring prior to fracture is close to that predicted for a perfectly plastic material. The larger values of mR for

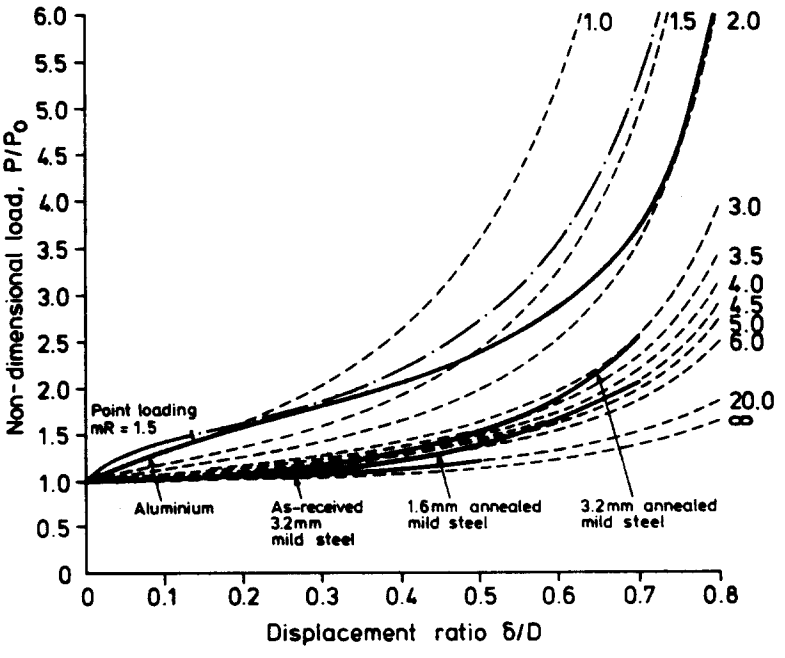

(a)

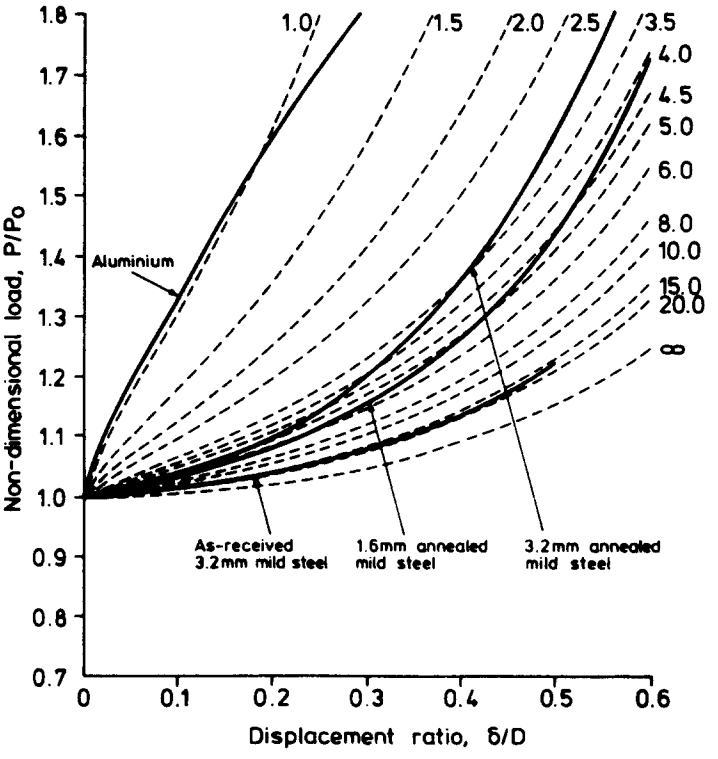

(b)

Fig. 8. Comparison between experimental data from flat plate compression tests and theory given in Ref. [11]. —— experimental data; ----theoretical curves for various values of mR. (a) Non-dimensional load up to 6.0; —|— point loading theory for $mR = 1.5$ up to point at which $\kappa_V = 0$; —·—notional flat plate theory for $mR = 1.5$ beyond point at which load line splits. (b) Non-dimensional load up to 1.8 to provide details of load variation at loads close to P_0.

the 3.2 and 1.6 mm annealed mild steel rings at smaller deflections reflects the effect of the plateau in the stress–strain curve following the jump from the upper to the lower yield point in producing a low mean strain hardening modulus in the early stage of plastic deformation. The transition to smaller mR values corresponds to the increasing influence of strain-hardening as reflected in a higher value for the mean hardening modulus in the later stages of deformation. Conversely the curve for aluminium has the opposite trend from lower to higher mR values as the deflection increases. This mirrors the reduction in the slope of the stress–strain curve as plastic deformation increases producing a decrease in the average strain hardening modulus in the region around H. However, as will be discussed below, the flat plate theory is somewhat in error for moderate deflections (< 0.3) for values of mR less than, say, 3.5 and this error reduces the range of mR values covered by the aluminium data.

The corresponding curves for point loading given in Fig. 9 show similar trends to those described in Fig. 8 with a tendency for the mR values governing the early deflection behaviour in the flat-plate test to persist to correspondingly higher deflections in the point loading case. The reason for this is clearly the lower levels of change in curvature which prevail in the critical regions (particularly H) for point loading as compared with flat-plate loading for the same deflection. This leads to lower strain levels and hence to behaviour which is governed by the mean strain hardening modulus values indicated by the early part of the flat-plate test results.

Relationship between flat-plate compression and point loading theories

In [11] the model established for the compression of a ring/tube between rigid, flat plates was simpler than that described above in the respect that only the regions around the hinges at the ends of the horizontal diameter, H, were replaced by plastic zones. Simple plastic hinges sustaining a constant bending moment M_0 were retained under the points at which the loads were applied. Since the level of deformation at these points is restricted compared with those points close to H and for other reasons outlined in [11,13], it was felt that the degree of approximation was reasonable, certainly if one's main interest lay in explaining the significant rise in load which occurs for deflection ratios in excess of 0.5 which was the main aim of [11]. Notwithstanding this, it is clear that when a ring is loaded in this way, within the context of a rigid-linear strain hardening theory, point loading is applied to the ring until the curvature under

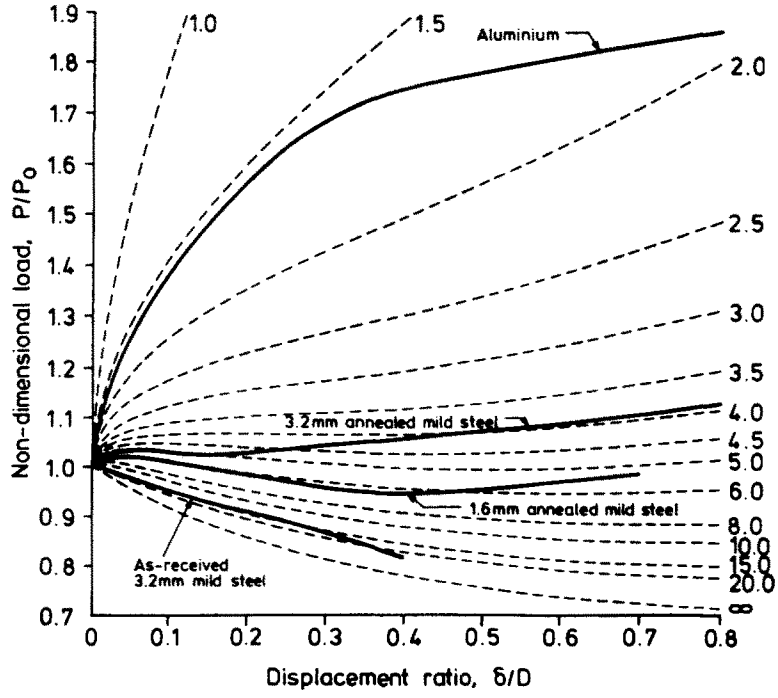

Fig. 9. Comparison between experimental data from point loading tests and theory. ——— experiments; ----- theory for various values of mR.

the point of contact has reduced to zero. Thereafter the contact point will divide and a flat contact region will develop. The initial phase during which the curvature reduces to zero is ignored in [11] and the flat contact begins to develop as soon as the load exceeds P_0.

Using Fig. 5 and 6(b) it is possible to extract from the results of the point load theory that part of the load-deflection curves covering the range of κ_v from 1 to 0. These are shown in Fig. 10 in conjunction with the original flat plate theory for several values of mR covering the range of mR values of interest. Clearly the major discrepancy between the two theories occurs for the smaller values of mR, the indications being that the flat plate curves should initially have a somewhat more rounded shape with a substantially steeper initial slope. The difference between the two theories becomes smaller the larger is mR. For mR greater than, say 3.5 the difference is probably negligible in the sense that, over the deflection range where differences occur, elastic effects are probably dominant.

The indications are that the growth of the plastic region around V does have a significant effect in flat plate compression for values of mR between 1 and 2 and that a better understanding of the behaviour of such rings would be achieved by utilising the analysis given earlier for the arc AV. This will not be attempted here. However, suppose one assumes that, once flattening has been achieved, the line of contact splits as described in [11] leaving a flat contact region. This will terminate at a section where the curvature is zero and where the bending moment is $M_f = M_0 + E_p I/R$. Extending beyond this will be a plastic region similar to AV in Fig. 3. As the

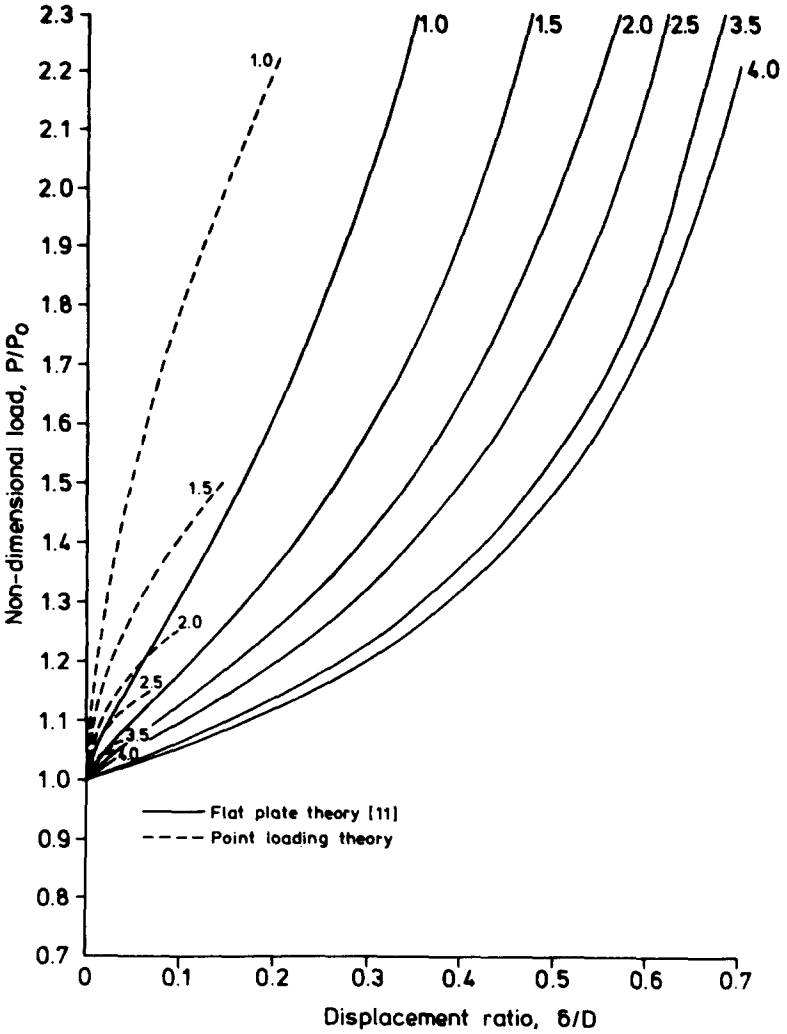

Fig. 10. Comparison between theoretical initial load-deflection curves for flat plate compression predicted by theory described in [11] and the point loading theory up to the load at which $\kappa_V = 0$ for values of mR between 1.0 and 4.0.

load increases the length of this region (or more precisely its horizontal project length) would reduce since the end moments remain constant. It is likely therefore that the discrepancy between the flat-plate theory and an amended one accounting for the length of the plastic region outside the flat contact region would reduce as the deflection increased. One might expect the sort of response exemplified by the dashed line for $mR = 1.5$ in Fig. 8(a) from which it can be deduced that the relevant range of mR values for the aluminium ring is within the range 1.5 to 2 rather than 1 to 2 as suggested by the simpler flat plate theory.

CONCLUSIONS

It has been shown that the role of strain-hardening is significant in the post-collapse response of rings loaded by opposed point loads. The unstable behaviour predicted by simple rigid-plastic theory largely dissappears for mR values frequently encountered for rings of the dimensions commonly found in components used for the purpose of impact energy absorption. The use of the plastica theory to analyse the plastic regions gives an insight into the effects of strain-hardening and the particular solution derived indicates certain limitations on the earlier theory derived for the compression of rings between flat plates.

Acknowledgements—The authors would like to express their gratitude to Miss A. Shipley for typing the manuscript and Mr. D. Bain for preparing the figures.

REFERENCES

1. G. Haaijer and B. Thurlimann, On inelastic buckling in steel. *J. Engng. Mech. Div., A.S.C.E.* **84** (EM2), 48 (1958).
2. S. C. Batterman, Plastic buckling of axially compressed cylindrical shells. *AIAA J.* **3**, 316–325 (1965).
3. G. Little, Collapse analysis of plates with strain hardening. *Int. J. Mech. Sci.* **9**, 561–576 (1981).
4. W. Johnson and S. R. Reid, Metallic energy dissipating systems. *Appl. Mech. Rev.* **31**, 277–288 (1978).
5. J. A. DeRuntz and P. G. Hodge, Crushing of a tube between rigid plates. *J. Appl. Mech., ASME* **30**, 391–395 (1963).
6. J. M. Alexander, An approximate analysis of the collapse of thin cylindrical shells under axial loading. *Q. J. Mech. Appl. Math.* **XIII**, pt. 1, 10–15 (1959).
7. W. Johnson, S. R. Reid and T. Y. Reddy, The compression of crossed layers of thin tubes. *Int. J. Mech. Sci.* **19**, 423–437 (1977).
8. J. F. Carney, III and R. J. Sazinski, Portable energy absorbing system for highway service vehicles. *Transportation Engng J. ASCE*, **104**, 407–421 (1978).
9. N. Perrone, Thick-walled rings for energy-absorbing bridge rail systems. Rep. No. FHWA-RD-73-49, Federal Highway Administration, Washington, D.C. (Dec. 1972).
10. A. R. Watson, S. R. Reid and W. Johnson, Large deformations of thin-walled circular tubes under transverse loading—I, II and III *Int. J. Mech. Sci.* **18**, 325–333, 387–397 and 501–509 (1976).
11. S. R. Reid and T. Y. Reddy, Effect of strain hardening on the lateral compression of tubes between rigid plates. *Int. J. Solids Structures* **14**, 213–225 (1978).
12. T. Y. Reddy and S. R. Reid, On obtaining material properties from the ring compression test. *Nuc. Engng Des.* **52**, 257–263 (1979).
13. T. Y. Reddy and S. R. Reid, Phenomena associated with the crushing of metal tubes between rigid plates. *Int. J. Solids Structures* **16**, 545–562 (1980).
14. W. Johnson, S. H. Ghosh, T. X. Yu and S. R. Reid, On thin rings and short tubes subjected to centrally opposed concentrated loads. *Int. J. Mech. Sci.* **23**, 183–194 (1981).
15. E. T. Onat, On certain second-order effects in the limit design of frames. *J. Aero. Sci.* **22**, 681–684 (1955).
16. S. R. Reid and T. Y. Reddy, Large deformation behaviour of thick rings under lateral compression. Proc. Conf. on Large Deformations, Delhi 1979, To be published.